Evidences of accumulation points in cascade regenerative phenomena observed in high voltage dc devices insulated by long vacuum gaps

Journal of Physics Communications

PAPER

Evidences of accumulation points in cascade regenerative phenomena observed in high voltage dc devices insulated by long vacuum gaps

N Pilan[1], S De Ambrosis[4], A De Lorenzi[1], M Cavenago[3], M Fincato[1], C Fontana[2], L Lotto[1], E Martines[1], R Pasqualotto[1], F Pino[2], F Rossetto[1], E Spada[1], S Spagnolo[1], P Veltri[1] and M Zuin[1]

[1] Consorzio RFX, (CNR,ENEA,INFN, Università di Padova, Acciaierie Venete Spa Association), Padova, Italy
[2] Università di Padova, Dipartimento di Fisica, Padova, Italy
[3] INFN/LNL, Lab. Nazionali di Legnaro, Italy
[4] ICMATE CNR, Padova, Italy

E-mail: nicola.pilan@igi.cnr.it

Keywords: cascade regenerative phenomena, electrode surfaces, neutrons sources applications

OPEN ACCESS

RECEIVED
30 May 2018

REVISED
20 September 2018

ACCEPTED FOR PUBLICATION
23 October 2018

PUBLISHED
5 November 2018

Abstract

Localized heating has been observed in unexpected positions on anodic surfaces in a multi-electrode device insulated by vacuum gaps. In double polarity experiments, a counter-intuitive behavior of current-voltage characteristic has also been observed. The phenomena could depend on a cascade effect of charged particles exchanged between electrodes and on a mutual correlation of particle trajectories between electrode surfaces occurring during the high voltage conditioning phase. Attractors regions ascribed to regenerative processes of charged particles between cathode and anode have been identified thanks to numerical simulations The position of the attractors depends only on electrode shape and the ratios of applied voltages. This finding suggests new perspectives in neutrons sources applications, where recurrent impacts of focused high energy hydrogen isotopes take place on solid hydride targets supported by metallic electrodes insulated by vacuum gaps.

1. Introduction

In the framework of the program for the construction of 1 MeV–16 MW negative-ion based neutral beam injector (NNBI) for ITER [1], an R&D activity on voltage holding in vacuum has been initiated in 2009. The activity is aimed at supporting the design, construction, and development of the NNBI accelerator.

The lack of a physical explanation of the vacuum breakdown phenomena has driven our group to investigate this topic by means of specifically designed experiments [2].

In vacuum or in any gas having a pressure lower than 10^{-4}–10^{-5} mbar, the free mean paths of molecules is much larger than the distance between the electrodes and thus the Townsend's discharge mechanism cannot explain the breakdown. In absence of magnetic field, the product between pressure and electrode gap length is so small that the classic Paschen curve [3] is not applicable. Therefore, under these conditions, the low-pressure gas between the electrodes cannot be considered the origin of the breakdowns, the electrode geometries, their material and the status of the surfaces necessarily become the causes that limit the maximum voltage holding.

A plenty of research activities have been documented concerning high voltage vacuum insulation in short vacuum gaps, up to few millimeters. However, only a limited number of works have been published considering long vacuum gaps, due to the obvious technical difficulties in the experimental set-up.

The breakdown behavior in the case of short vacuum gaps is well described by the field emission based theories [3, 4], but this is not valid in the case of long vacuum gaps.

In case of short vacuum gaps, the breakdown is characterized by the existence of a maximum electric field E_B. Such field depends on the electrode materials and on the status of the cathodic surface. In case of plane parallel electrode the maximum voltage holding V_B is proportional to the gap length d, and thus $V_B = d \cdot E_B$.

The latter equation is not valid in the long gap cases where $V_B \propto d^{\alpha}$, with $\alpha = 0.3 \div 0.5$[5] [6]. Such loss of direct proportionality between the maximum voltage and the gap length suggests that an interaction between opposite electrodes determines V_B: the 'local' status of the metal-vacuum interface of only one electrode is no longer sufficient to properly describe the initiation of the discharge.

In both cases (long and short gaps), it is usually necessary an *in situ* treatment, called 'high voltage conditioning', to achieve the maximum withstanding voltage for the configuration under test [3]. The conditioning in dc is typically done by applying small discrete voltage steps repetitively and waiting for the system to achieve a stationary condition before increasing the voltage again, conditioning can also be done by using pulsed voltages in a similar manner. The high voltage conditioning is a process associated to and characterized by intermittent microdischarges, usually accompanied by x rays and gas emission, that leads to the safely quench of further possible source of breakdowns. As a result of this process, both microdischarge and breakdown thresholds voltages are improved [7].

Several investigations have been carried out to understand the physical mechanisms governing the conditioning process. In case of long vacuum gaps, it is still not completely clear which electrode (anode, cathode or both) is subject to the surface modification occurring during the conditioning procedure.

Moreover, the exact role of the background gas pressure, which can improve, within certain limits, the voltage holding of a system insulated by vacuum [6] is also unclear.

A first analysis of the phenomena initiating the breakdown in vacuum would suggest the existence of a threshold in the electric field or in the triple product (electric field on anode surface and cathode surface and applied voltage) [8] are the causes initiating the breakdown respectively for short and long vacuum gaps. In both cases the observations reported in the present paper highlight the importance of a global approach; the latter would require also analyzing the areas candidates to concentrate the flux charged particle exchanged between electrodes. Such phenomenon could induce power dissipation in unexpected positions on the electrode surfaces until limiting the voltage holding performances.

This issue could imply a severe degradation of the electrode surfaces when the high voltage (>100 kV) power supplies can deliver also high currents (>1 A) and the electrode surfaces are not actively cooled, e.g. the electrostatic accelerator or the beam source vessel of the ITER NBI injector could be damaged during the conditioning phase if the phenomenon is not monitored and the high voltage is raised quickly.

The present paper deals with the findings observed during the high voltage conditioning tests carried out at the High Voltage Padova Test Facility (HVPTF). HVPTF is a laboratory designed to carry out high voltage tests in vacuum in dc up to 800 kV. It has been built in collaboration between the Consorzio RFX, the Padova University and the INFN laboratories it has been equipped by several diagnostic systems to monitor the characteristic of discharges and radiation occurring during high voltage tests in vacuum [9, 10].

2. Experimental setup description and measured quantities

The system consists of a cylindrical vacuum vessel (1.2 m in diameter and 2.4 m long), connected to a pair of power supplies. The vessel is pumped by a turbo-molecular vacuum pump having a pumping speed of 1000l/s in N_2. In figure 1, a scheme representing the setup and the measured quantities is shown.

Each electrode is polarized respectively by a negative and by a positive high voltage Cockcroft-Walton (CW) power supply. Both units are rated for 400kVdc 1 mA; the two units are in series in order to obtain a total voltage of 800 kV between the electrodes under test. A 15 MΩ resistor is connected between each electrode and the CW multiplier to limit the breakdown currents.

Each high voltage power supply can measure the voltage, (V+ and V−), and the currents, drained by the electrodes (I+ and I−). The signals have a bandwidth of about 1 kHz.

The difference between I+ and I− is the current directed towards the vacuum chamber, which sometimes acts as a third electrode. This happens although the distance between the electrodes under test and vacuum chamber wall is 600 mm and no electric field concentrations are present. The signals from the power supplies (V+, V−, I+, I−) and the pressure signal p of a Bayard Alpert hot cathode gauge (Oerlikon ITR90) are sampled synchronously at 100 Hz during the tests.

An Inficon Transpector TSP-TH100 Residual Gas Analyzer (RGA) is adopted to measure the composition of the gas desorbed from the electrode surfaces during the experimental sessions. The RGA is connected directly to the vacuum chamber; no differential pumping systems have been used.

The Equivalent Dose Rate [μSv/h] (EDR) of the x-ray produced during the experiments is measured by a Berthold Dose Rate Probe LB 1236 located outside the vacuum chamber, 1 meter from the chamber wall.

An Infra-Red Camera (IRC) FLIR A655sc 25° is dedicated to monitoring the electrode temperatures during the tests. The spatial resolution of the camera is 1.5 × 1.5 mm^2; each frame is recorded at 50 Hz.

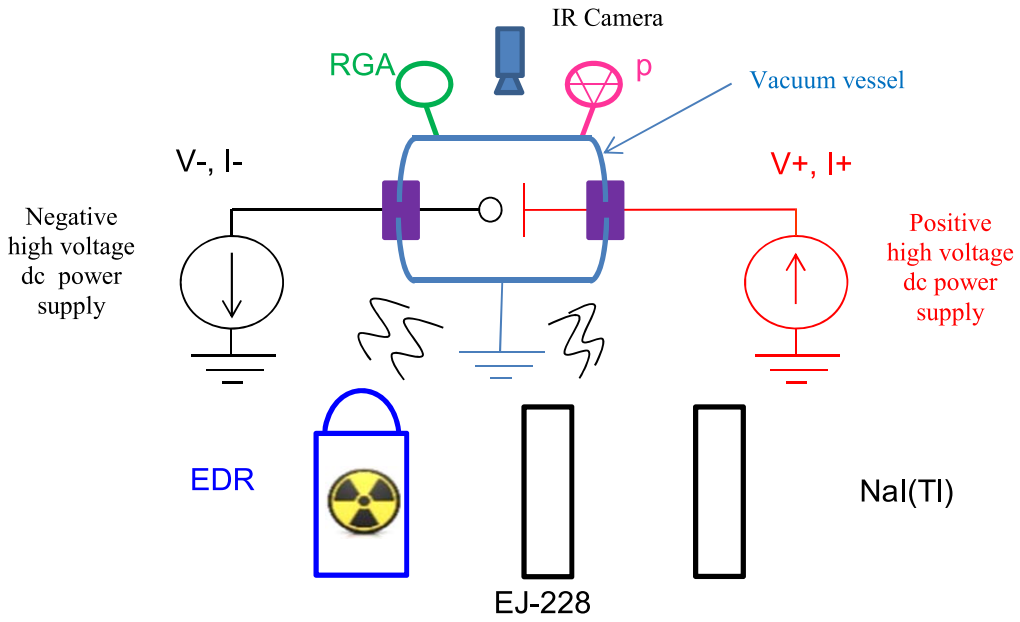

Figure 1. Setup scheme and measured quantities. V+, I+ and V−, I− are the measured voltage and currents respectively for the negative and the positive power supply. Residual Gas Analyzer (RGA) is the mass spectrometer. p is the pressure gauge. EDR represents the x- (and gamma) ray dosimeter to measure the Equivalent Dose Rate. The EJ-228 and NaI(TI) represent the scintillator probes.

An acquisition system has been implemented and calibrated to detect the energy spectrum of the x-ray emitted during the experimental sessions. The system consists of two scintillators: a NaI(Tl) inorganic scintillator, 3 inches in diameter and 2 inches thick, and a EJ-228 organic scintillator made by Polyvinyltoluene (PVT), 2 inches in diameter and 2 inches thick. Each scintillator is coupled with its own photomultiplier, they are positioned in air, outside the vacuum chamber, 1 meter far from a glass window DN 100, 5 mm thick. Both units are connected to a CAEN DT5720B multichannel digitizer, energies and times of each single photon detected is recorded up to a maximum rate of 350 kHz.

The objects exposed to vacuum are the two electrodes under test, the inner chamber wall (made of stainless steel), the surface of insulators, covered by glass, and the exposed surface of the vacuum sealing which can be made of copper or rubber elastomer (Viton^{TM}). No baking systems are present. The electrodes under test are sustained by cantilever brackets; the latter are composed by a cylindrical stainless steel tube connected to an alumina feedthrough.

During the experimental campaign described in this paper, two AISI 304L electrodes have been tested, both electrodes have been manufactured by lathe machining.

The electrode used as a cathode is a sphere 40 mm in diameter, while a planar electrode 108 mm in diameter is the anode. The minimum vacuum gap length between the electrodes is 30 mm along the axis of the system, as shown in figure 3.

A surface roughness Ra better than 0.8 μm has been obtained on both electrodes by using abrasive papers. The papers are a polyester film with a deposition of abrasive grains of aluminum oxide. No lapping pastes have been adopted to treat the electrode surfaces. After finishing, both electrodes have been cleaned in a water solution by an alkaline detergent by using an ultrasonic bath; the electrodes have than been wiped by clean cloths and acetone.

A picture of both electrodes during the high voltage test is shown in figure 2.

A finite element analysis has been carried out to calculate the electrostatic field map of the configuration under test. For the calculation, the Laplace equation has been solved using the commercial code Comsol®.

In figure 3, the result of the electrostatic 2D axial symmetric analysis is shown. The electric field map in vacuum is visualized in terms of equipotential lines and electric field strength. In the simulation the applied voltages are −100 kV at the sphere and +100 kV at the plane electrodes.

3. Experimental procedure

At the HVPTF laboratory, the conditioning procedure can be carried out applying voltage manually in both units or automatically. The voltage can be gradually raised step by step manually at the best vacuum level

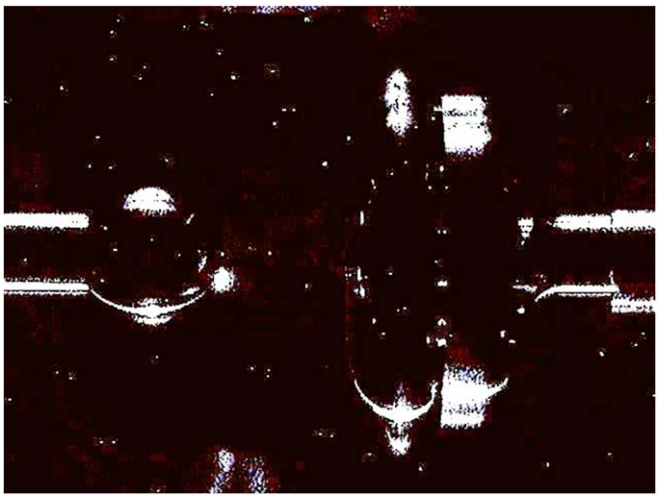

Figure 2. Picture of the axial-symmetric electrodes during a microdischarge, spherical cathode (left) and planar anode (right). The white spots are the effects of the x-rays on the pixels of the visible camera adopted.

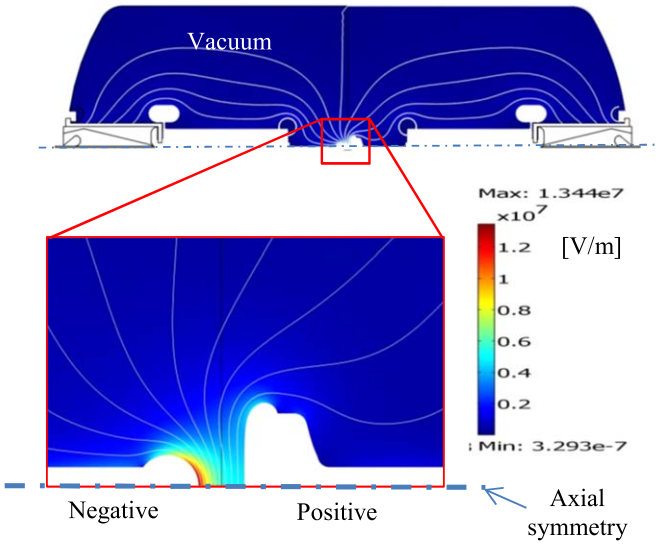

Figure 3. Electrode geometry, vacuum gap length 30 mm, electrostatic field distribution at 200 kV (V−=−100kV and V+= +100 kV) applied between electrodes.

reachable by the system ($p < 3. \times 10^{-7}$ mbar). This technique is one of the most consolidated methods for improving the voltage holding of a device insulated by vacuum [3].

Alternatively, a fully automatic procedure can be adopted to apply the DC voltage to the electrodes under test: voltage is raised symmetrically in both power supplies.

The automatic procedure was adopted in this case, in order to obtain more reproducible experimental results.

The automatic conditioning procedure is schematically represented in figure 4. The voltage V is applied at constant speeds: K_{FAST}, K_1 and K_2 within specified voltage ranges which are respectively: $0 < V < V1$, $V1 < V < V2$ and $V > V2$. A breakdown is characterized by a quick collapse of the voltage to ground in few microseconds. A breakdown can involve one of the power supplies or in both; when a breakdown happens, the reference voltage is forced to zero in both units. Finally, a time delay Δt is applied before restarting the automatic rise of the voltage.

At the occurrence of the i^{th} breakdown, the corresponding voltage $V_{BD}i$ is recorded and the parameters V_1 and V_2 are updated as follow: $V_{2\,i+1} = V_{BD\,i}$ and $V_{1\,i+1} = 0.9^{*}V_{BD\,i+1}$,

In the preset experimental campaign the following parameters have been adopted for both power supplies: $K_{FAST} = 25\ \text{kV min}^{-1}$, $K_1 = 0.5\ \text{kV min}^{-1}$ and $K_2 = 0.25\ \text{kV min}^{-1}$. $\Delta t = 2$ min $V_{BD\,1} = 80$ kV.

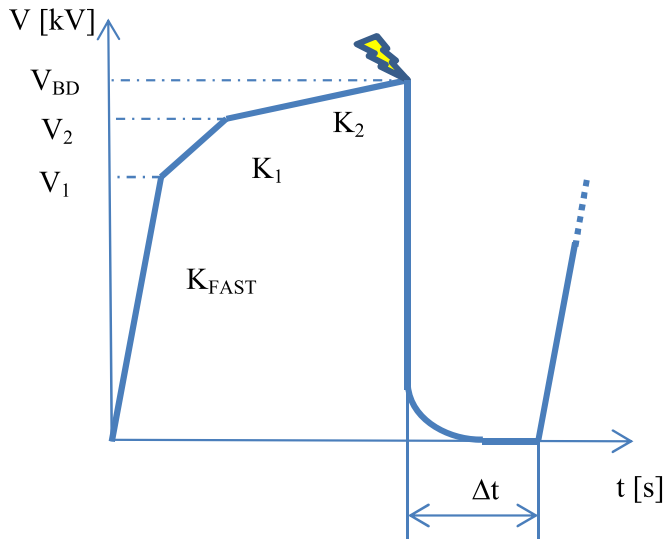

Figure 4. Automatic conditioning procedure parameters.

The maximum currents Imax+ and Imax− can be set in each power supply in the range 0–1 mA. When I = Imax, in one of the power supplies, the 'current control' mode is triggered,,, the automatic conditioning procedure is suspended and the control is driven by the single unit where I = Imax. During this occurrence both reference voltages are kept constant, the reference voltages can be different from the measured voltages V+ and V−. The current control mode usually occurs at high voltage if the electrodes are not cleaned properly, and is characterized by a progressive increase of microdischarge frequency up to a continuous release of charges and material from the electrode surfaces.

During the current control mode, the high voltage conditioning proceeds although V+≠V−.

4. Experimental results

As explained in the previous chapter, the measured quantities are the currents I+ and I−, the EDR, the pressure, the voltages V+ and V− and the x-ray counts. In figure 5, the time evolution of the recorded quantities is shown during the application of the automatic conditioning procedure for a typical experimental session. A total number of 48 breakdowns have been recorded in this case. A saturation value of the breakdown voltage has been achieved at 320 kV between the electrodes.

During the whole session, a relatively high contribution of I+ with respect to I− has been observed. That suggests a not negligible interaction between the positive power supply and the vacuum vessel.

The composition of the gas released during the micro discharge occurrence is shown in figure 6. Molecular hydrogen and nitrogen, water and carbon dioxide are the main gas species emitted during microdischarges. The RGA signals have time evolution compatible with the pressure signal shown in figure 5.

During the high voltage test, the IR camera did not show any appreciable temperature variation on the electrode surfaces. Nevertheless, a temperature rise in the metallic cantilever structure connected to the positive power supply has been observed. Figure 7 shows the temperature map after a microdicharge occurrence. The microdischarges lasted for 20 s, while the power generated by the positive power supply was about 160 kV × 0.1 mA = 16 W.

An increment of +5 °C has been observed only on the support of the anode as reported in figure 7. No other points with a similar temperature rise were found.

Other two sessions were done after the one shown in figure 5: the same automatic procedure was used and the vacuum system wasn't turned off. The voltage holding didn't improve and the same behavior of the system was observed.

An additional session was carried out by applying voltage as shown in figure 8. The automatic conditioning procedure was suspended for t > 1330 [s]. The voltage between electrodes was kept constant at 320 kV until the occurrence of a breakdown at t = 2380 s. The voltage of both power supplies were raised symmetrically again up to −160 kV and +160 kV, then they were kept constant for 2850 < t < 3270 [s] since the micro-discharge activities disappeared.

The interesting part of the session occurs at t > 3270 s, when only the voltage of the negative power supply was manually decreased. The time evolution of the total voltage between the electrodes is shown in the last plot

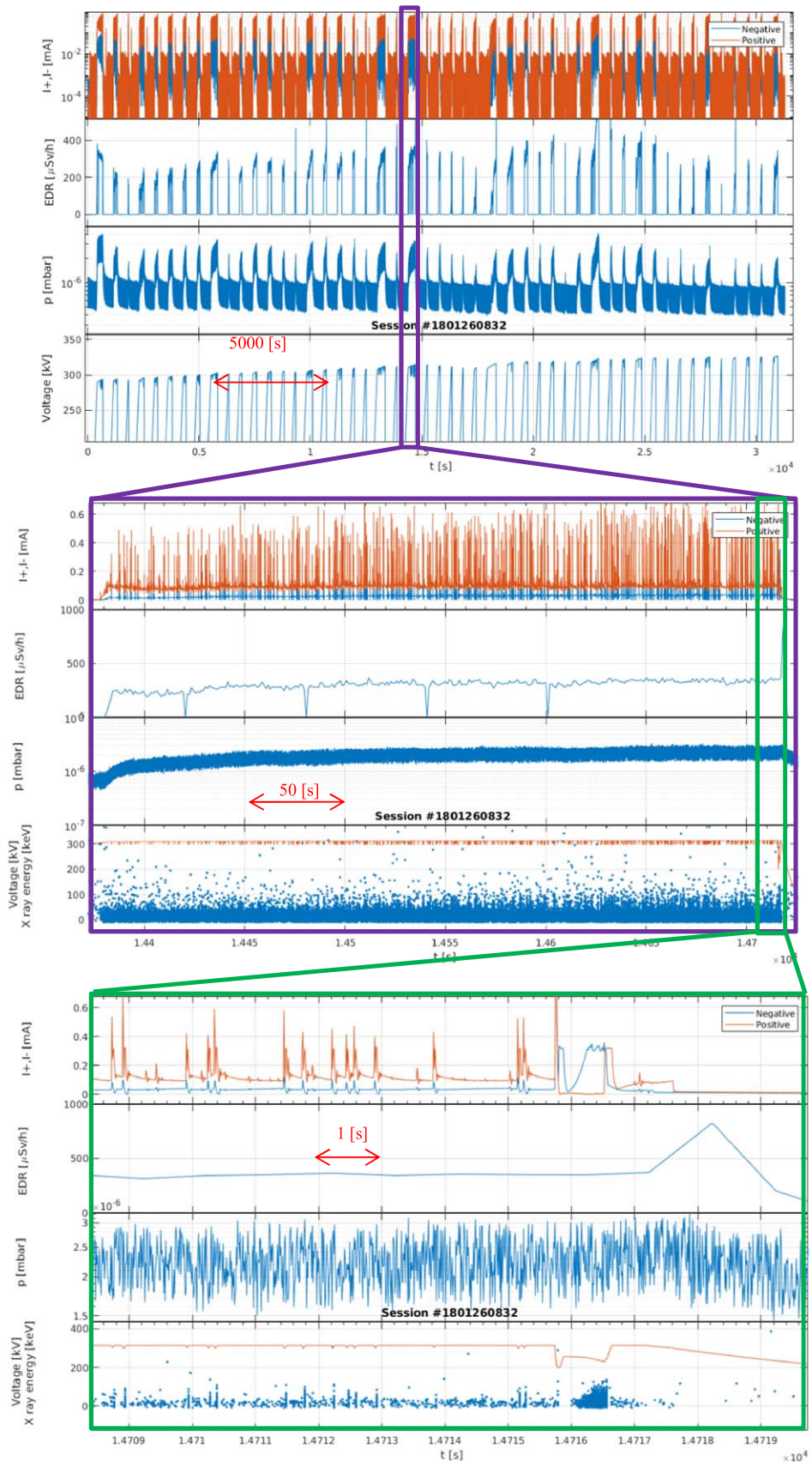

Figure 5. Currents, EDR, pressure, voltage and x-ray counts of EJ-228 scintillator versus time in session #1801260832, session controlled by the automatic conditioning procedure. The delay of the EDR record depends on the post processing of the data buffer.

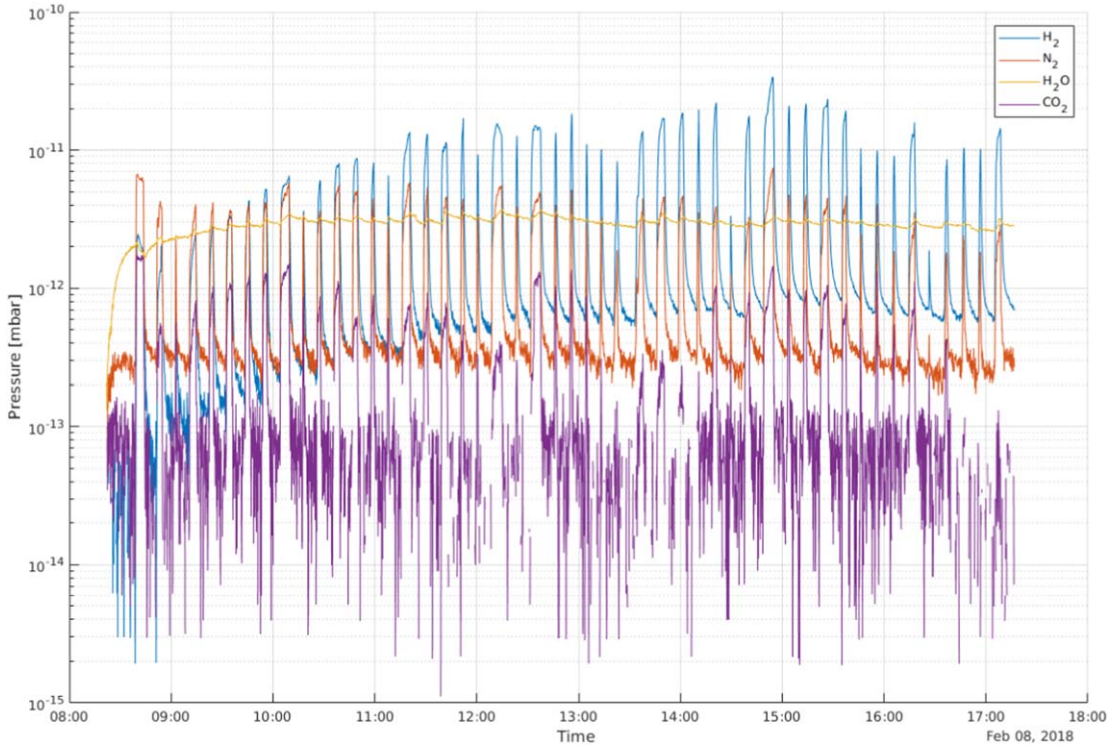

Figure 6. RGA signals versus time in session #1801260832, session controlled by the automatic conditioning procedure.

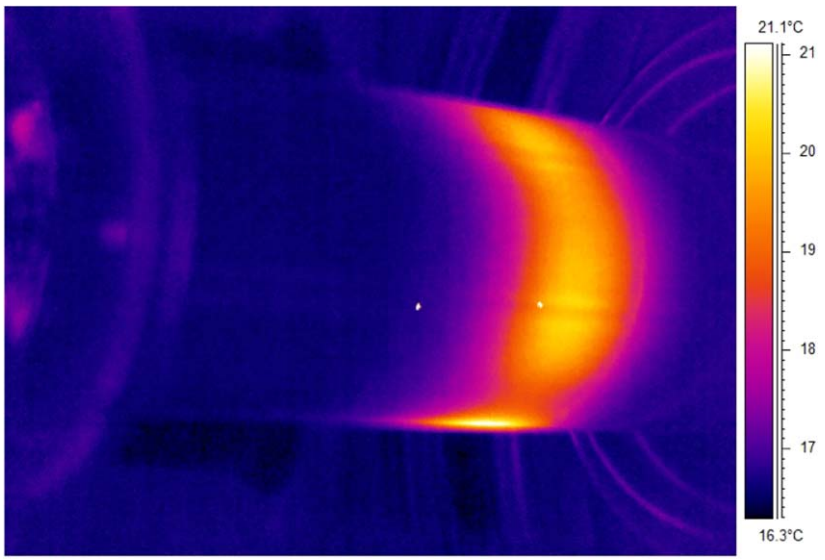

Figure 7. IR camera picture of the stainless steel (cantilever) arm connected to the positive power supply and supporting the planar electrode.

of figure 8. The microdischarge onset occurred when the voltage of the negative power supply was decreased from 160 kV to 155 kV. At constant voltage, micro-discharges tended, as usual, to extinguish until a further step-down voltage was applied.

These series of micro-discharges were accompanied by the local heating of the anodic support as observed in the previous experimental session #1801260832 (see figure 7).

The dynamic response of the x-ray counts detected by the PVT scintillators is in agreement with the other measured quantities but the interpretation of the energy associated to each count is not straightforward. The energy recorded is mainly the result of the Compton scattering [11] interaction of the primary photons coming from the experiment and the scintillator material. The energy of the primary photons is due to the

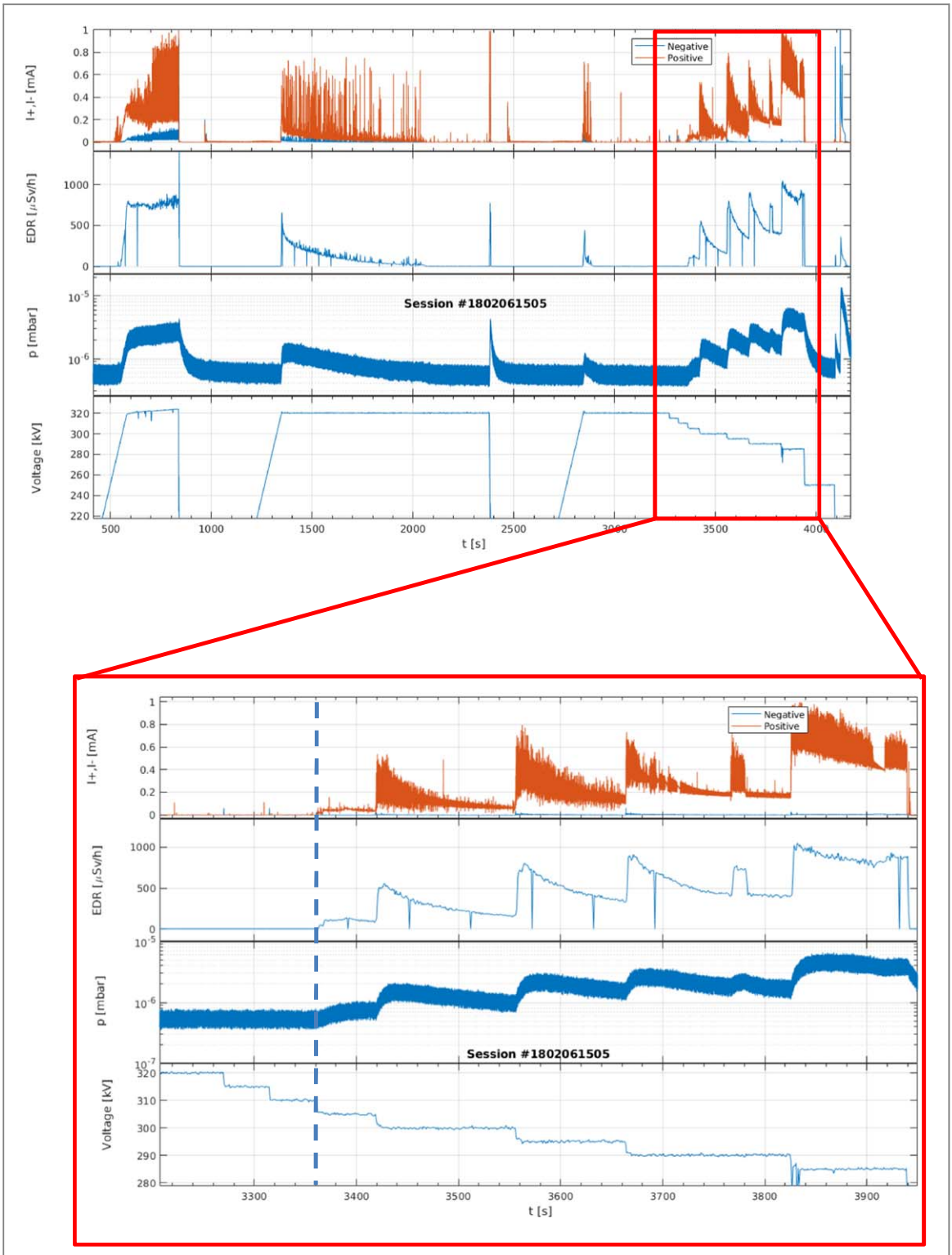

Figure 8. Currents, EDR, pressure, voltage versus time in session #1802061505. The dotted lines highlights the restart of the microdischarge activity during the stepdown voltage of V−, V+ was kept constant at 160 kV.

Bremsstrahlung radiation of electrons decelerated on anode. Their energy distribution can be described by the Kramer's law [12]. This diagnostic system and the measurements interpretation will be discussed in detail in [9, 10].

The energy spectra recorded in the time windows $W_{i=1,2,3}$ of figure 9 are shown in figure 10. Note that the counts $C_{i=1,2,3}$ are respectively 735, 205 and 162 for the same time window of 4 s.

After several tests were executed changing the gap length and the electrode geometry, while the power supply polarity kept unaltered, a couple of annular brown traces have been observed on the vacuum chamber inner wall, in front of the anodic support (see figure 11).

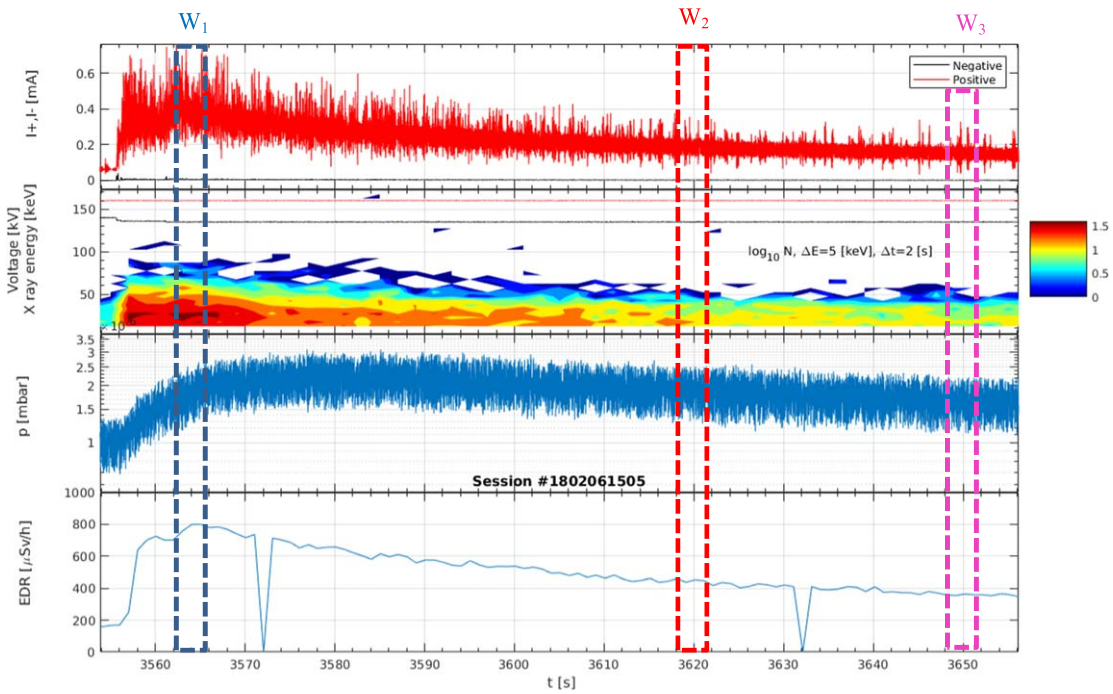

Figure 9. Currents, voltages, x-ray spectrum, pressure, EDR as function of time.

A reduced amount of material has been also deposited in the insulator indicated in the point P of figure 12

A sample have been cut from the insulator and analyzed by the Energy Dispersive x-ray Analysis (EDX). In figure 13 the sample and the analyses results are shown.

The brown layer composition is compatible with Iron and Chromium, the layer appears very thin ($t_k < 1\ \mu$m). Fe and Cr are fully consistent with the composition of the stainless steel which is the sole metal adopted for the vacuum chamber and for the electrode under test. The most obvious conclusion is, thus, that the brown traces are produced by material coming from the stainless steel anodic support.

5. Numerical analyses and discussion

The most evident aspect, concerning the results so far reported in the previous section, is that a spurious phenomenon has influenced the high voltage tests. The microdischarge activity has involved mainly the vacuum vessel and the positive power supply rather than the two electrodes shown in figure 2, although they were separated by the shortest gap length and subjected to the largest difference of electric potential.

The unexpected behavior of the system has raised two fundamental questions concerning the position of the local heating shown in figure 7, as well as the explanation of the unexpected phenomenon highlighted in figure 8 characterized by the occurrence of microdischarges during the step down voltage of V−.

A steady interchange of charged particles and photons between cathode and anode is one of the hypothesis proposed in the past literature [13] to explain breakdown events over long vacuum gaps, because of the inadequacy of the (sole) field emission theory at high voltages (>50 kV).

Adopting this hypothesis, it is easy to demonstrate that breakdown should occur when the following relation is satisfied

$$A \cdot B + C \cdot D > 1 \tag{1}$$

being the coefficient A the number of positive ions produced by one electron impact, C the number of photons produced by one electron deceleration (on the anodic surface), B the number of secondary electrons produced by one positive ion impact and D the secondary electrons produced by a photon (at the cathodic surface).

Direct measurements of coefficients A and B carried out by the same authors [13] and moreover by [14] would not immediately support the validity of (1). Nevertheless, the same type of analysis should be carried out also for the coefficients C and D so as to have a complete benchmark of this assumption with the reality.

The energy spectra shown figure 10 has been measured using a plastic scintillator material, so photons interact by single Compton scattering rather than photo-absorption. This means that full energy peaks are not directly observable. Moreover, it is plausible that the distribution of photons generated by the Bremsstrahlung radiation of mono-energetic electrons impinging the anodic surface follows the Kramer law. Assuming the

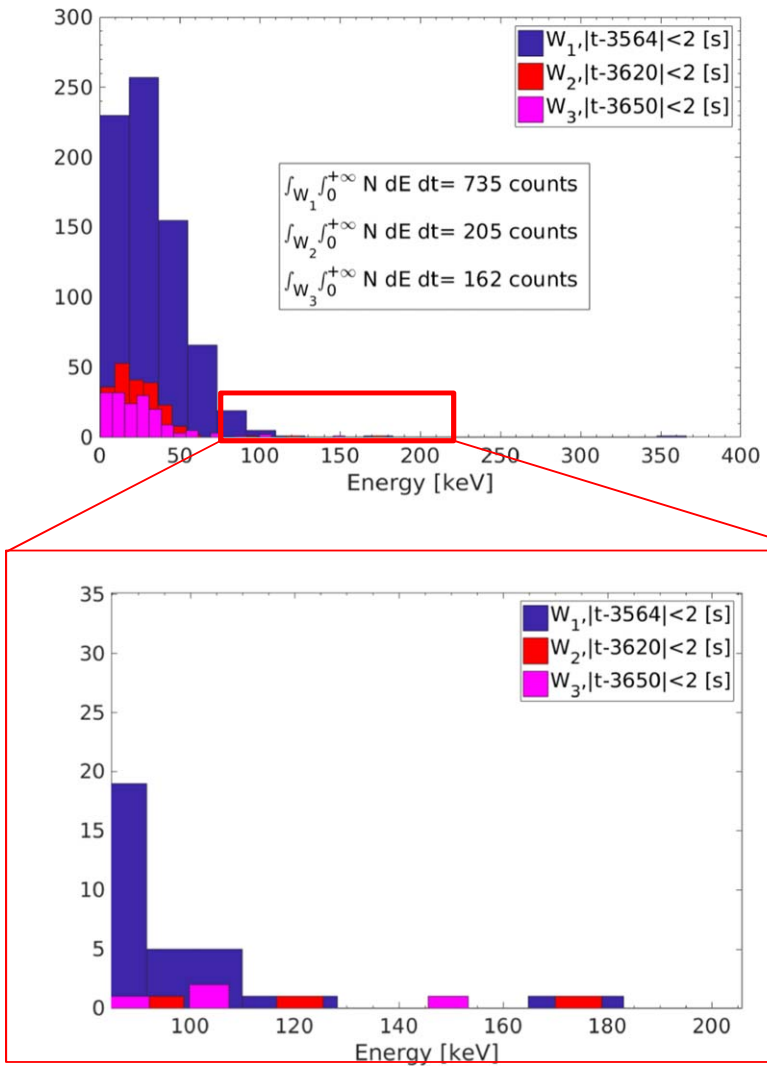

Figure 10. X-ray spectrums in time windows W_1, W_2 and W_3 as shown in figure 12.

Compton scattering distribution according with the Klein–Nishina equation [15], it is possible to reconstruct, by means of a Monte Carlo 1D algorithm, the shape of the spectra shown in figure 10,

The numerical results are reported in figure 14. The results of the simulations are consistent with the general trend of the experimental results, which exhibits an energetic spectrum having negative slopes with a maximum energy according with the accelerating voltage.

The number of the counts of the simulations is proportional to a coefficient which could be obtained by specific tests accelerating a known electron current toward the anode and measuring the rate of the x-ray counts detected by the scintillator.

The number of counts C_i in the time windows $W_{i=1,2,3}$ of figure 9 decreases without keeping the proportionality with the measured current I+, actually in W_1 $<I_1+> = 0.40$ mA, W_2 $<I_2+> = 0.19$ mA and W_3 $<I_3+> = 0.15$ mA while $C_1 = 735$, $C_2 = 205$ and $C_3 = 162$, the respectively ratio are: $C_1/<I_1+> = 1.84e06$ [1/A], $C_2/<I_2+> = 1.08e06$ [1/A], $C_3/<I_3+>=1.08e06$ [1/A].

The measured currents, I+ and I−, are respectively the sum of electrons and negative ions currents directed toward the anode and the opposite contribute due the positive ions coming from the anode. A progressive reduction of the ratio $C_i/<I_i+>$ could be justified considering a progressive reduction of the electron current being the sole type of charge particle able to generate x-rays. In this view, the microdicharge activity would lead toward a progressive reduction of the electron extraction from the cathodic surface, probably due to not negligible contribute of the extracted ions from the anodic surface.

The peculiar spatial distribution of the emission sites on the electrode surfaces, shown in figure 7, has been analyzed thanks to the idea proposed in [16] where a mutual exchange of charged particles, with opposite sign, is simulated between electrodes having a generic shape. The numerical simulations reported in [16] reveal the

Figure 11. Inner wall of the HVPTF vacuum vessel: two circumferential stains have been progressively appeared during the execution of the high voltage tests.

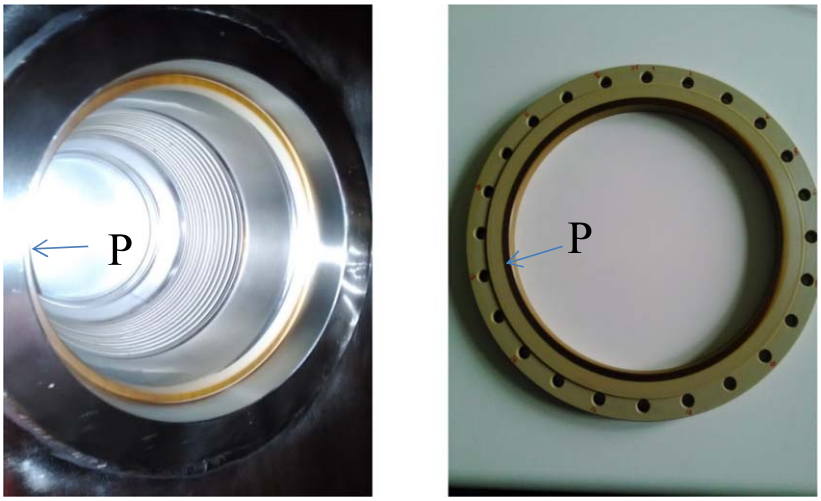

Figure 12. Material deposited on insulator from anode.

existence of specific points on the electrode surfaces able to concentrate the charged particle exchanged between electrodes.

A set of numerical simulations considering the HVPTF geometry has been carried out, following the same approach, to justify the observations described in the previous section.

The trajectories of positive charged particles, uniformly distributed on the anodic surfaces, have been integrated considering the 2Daxialsimmetric electrostatic field map reported in figure 3. The axial-symmetric domain assures the conservation of the angular momentum. The starting positions of the charged particles have been located on the anode surface on the right hand side. The integration of the equation of the motion starts assuming an initial null speed: this assumption assures trajectories having a radial path located in a plane at constant azimuthal coordinate. The trajectory stops when a charged particle hit an electrode, than the sign of the charge is changed and a new trajectory is integrated. The process has been repeated up to a condition characterized by a stationary mutual-exchange of trajectories. In this geometry, twenty iterations are necessary to converge toward the final configuration. The trajectories have been grouped and exchanged only between two

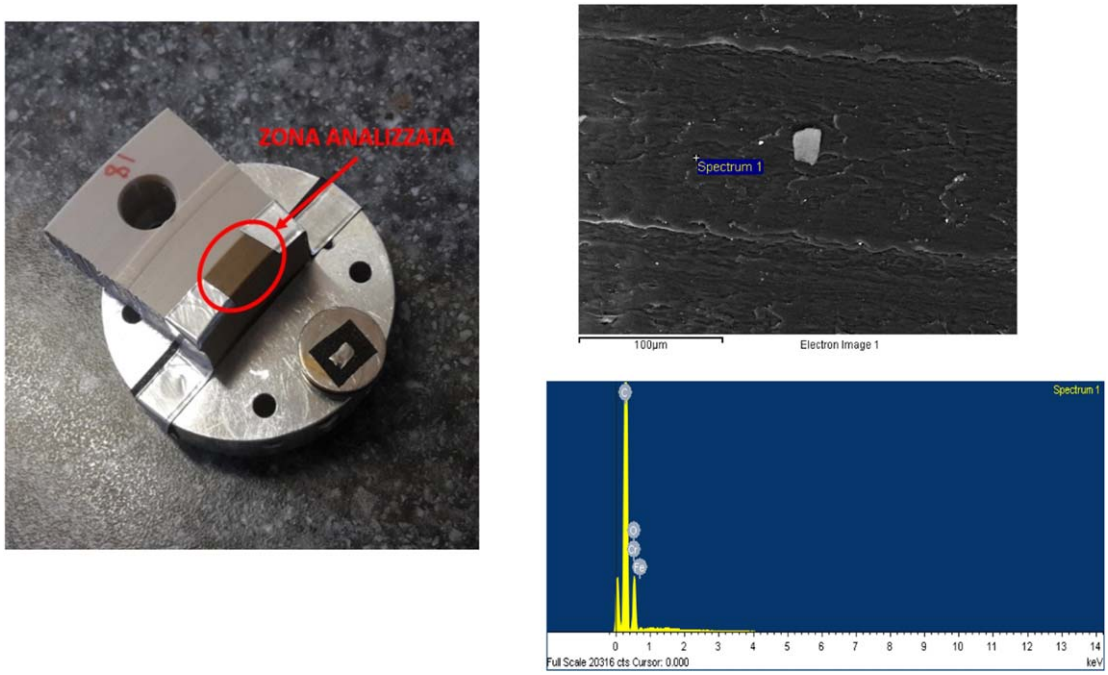

Figure 13. Sample and results of the EDX analysis.

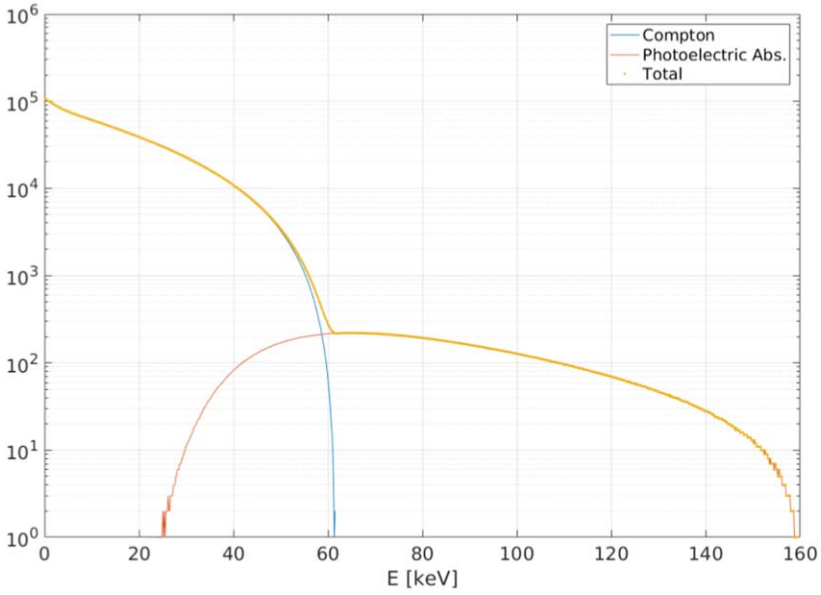

Figure 14. Results of the Monte Carlo calculation: reconstruction of the x-ray spectra recorded by the EJ-228 scintillator due to the bremsstrahlung radiation of a monoenergetic electron beam of 160 keV impinging the vacuum vessel.

points A and C, respectively on the anode support and the cathodic surface of the vacuum vessel. Such points are called discharge attractors as referred in [16].

It is possible to demonstrate that the trajectory path of a charged particle in an electrostatic (irrotational) field, assuming classic motion and zero initial velocity, depends only on the shape of the domain and the ratio of the applied voltages (in case of multi-electrode system). A concise demonstration of the independence of the trajectory upon mass, charge and even gap voltage is reported in Appendix.

Under such conditions the attractor locations depend only on the shape of the electrodes and on the ratio between the applied voltages.

In this simulation the ratio $\alpha = \mathrm{V}-/\mathrm{V}+$ between the applied voltages is 1 and the ratio m/q can be arbitrarily chosen. The first three and the last (20th) iterations are shown in figure 15: the trajectories of the

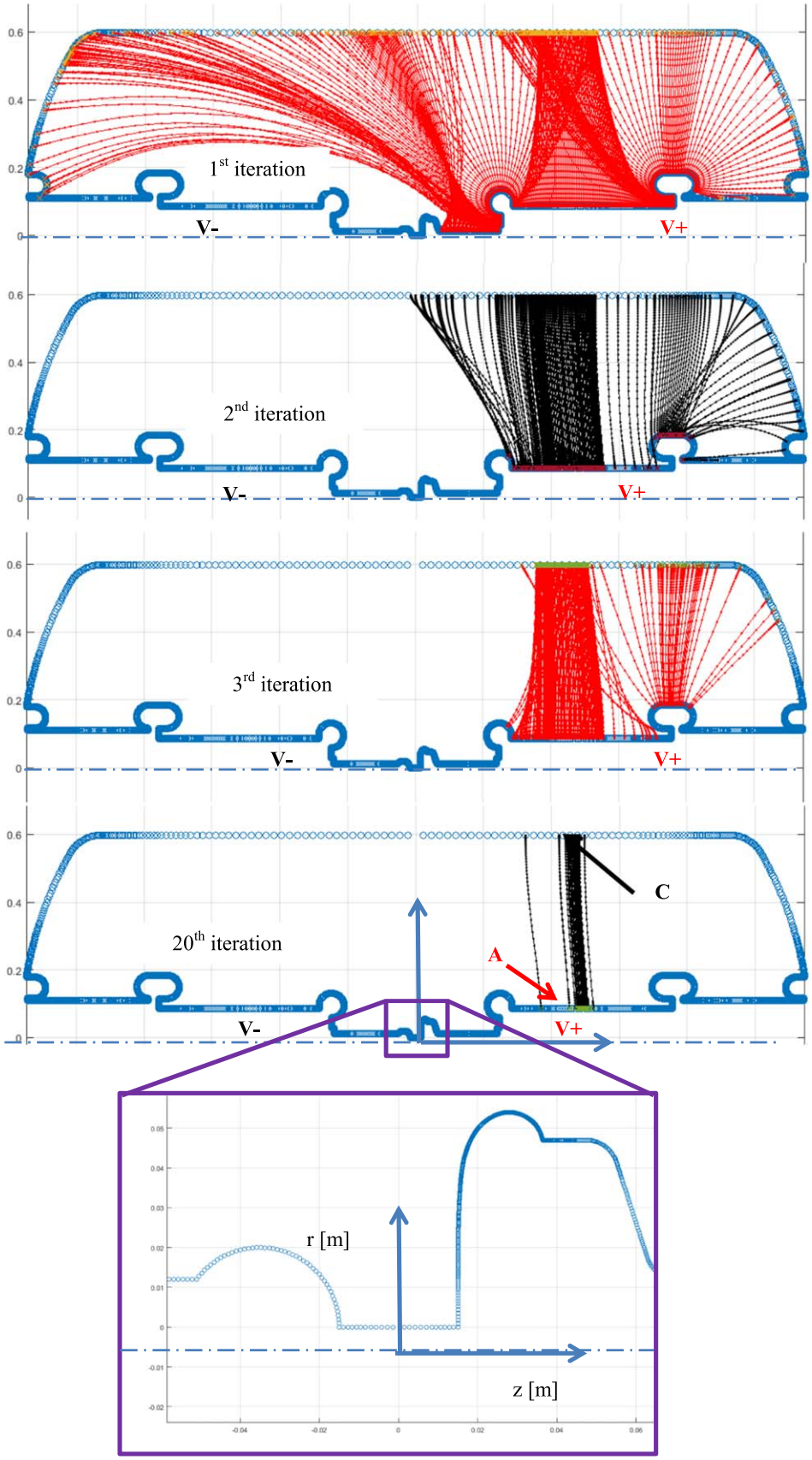

Figure 15. Cascade of trajectory paths in case of $\alpha = 1$ (V+ = V−), red and black trajectories refers respectively to positive and negative charged particles, a magnified view of the electrodes shown in figure 3 is reported in the bottom part of the picture.

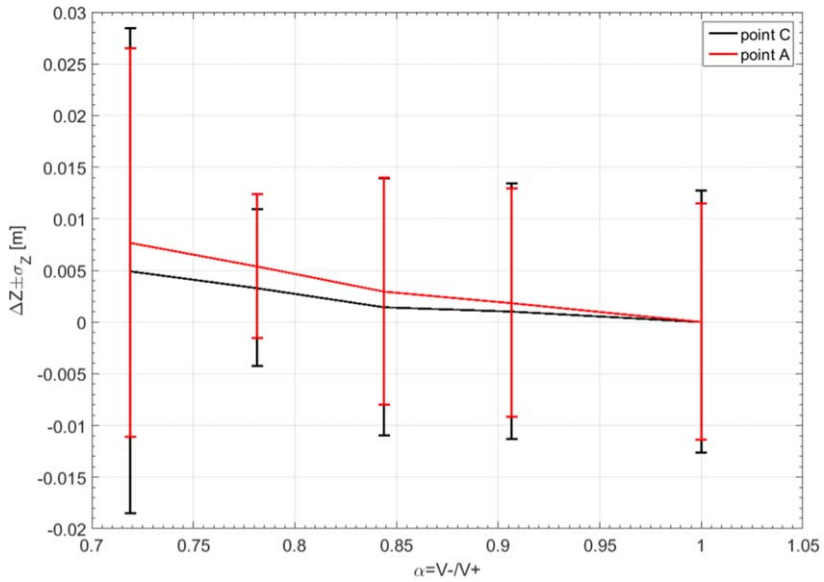

Figure 16. $\Delta z \pm \sigma z$ versus α for points C and A respectively in black and red color.

positive charged particles are in red, while the ones of the negative charges are in black. The trajectories converge toward the attractor point A on the metallic support at V + voltage, corresponding to the hot spot area shown in figure 7, and toward the attractor point C at the cathodic surface on the vacuum vessel wall.

A systematic set of numerical analyses have been done at different voltage ratio α (=V−/V+). The results in term of trajectory paths are similar to those shown in figure 15, except for the final positions of the attractor points C and A which exhibit an average displacement of less than 30 mm reducing α from 1 to 0.72.

The z-coordinate z_A and z_C respectively of the attractor points A and C (see figure 16) have been defined as the average z-coordinate of the end points of each trajectory, while the spreads of the same z-coordinates σ_{zA} and σ_{zC} have been defined considering the corresponding standard deviation.

Figure 16 shows the relation between the displacement $\Delta z = z\text{-}\, z_{(\alpha=1)}$ and α, both for the point C and for the point A; the error bars are equal to σ_z.

Starting from a symmetric distribution of electric potentials (α =1) a displacement of about +0.4 and +0.8 mm occurs respectively for Z_C and Z_A passing to $\alpha = 155/160 = 0.96$, this ratio is the condition highlighted by the dotted line in figure 8 corresponding to the micro discharge onset obtained decreasing only V−.

The numerical analyses above described adopt a very simple model, based on restrictive hypotheses of a null initial velocity. Nevertheless, the estimation of the displacements ΔZ_C and ΔZ_A could help to understand new aspects concerning the voltage conditioning in high vacuum, i.e. in case of a system partially conditioned if Z_C and Z_A are perturbed up to few tenths of millimeters the system keep unaltered its state; on the other hand, in case of larger perturbations, additional conditioning and adaptation of the interface vacuum-metal are necessary. The analysis of these experimental results does not show sufficient evidences to discriminate if the micro discharge precursors can be attributed to ΔZ_C rather than ΔZ_A. Nevertheless, dedicated high voltage tests (with double polarity) could be designed in order to discern this important aspect. The analyses of experimental results in the following situation: $\frac{\partial(\Delta z_C)}{\partial \alpha} = 0$ and $\frac{\partial(\Delta z_A)}{\partial \alpha} \neq 0$ (or vice versa) should be sufficient to understand the asymmetric behavior of cathode versus anode during the high voltage conditioning in vacuum.

The electrode configuration discussed so far has symmetric domain boundaries $r(z) = r(-z)$, except for the region between the electrodes under test, thus another couple of attractor points exists on the support on the left. However, as anticipated in the previous section, no detectable temperature rise has been observed on the structure connected to the negative power supply neither on the vacuum chamber wall. This is confirmed by the generally small current I- recorded during the experimental sessions. This asymmetric behavior depends on the different role assumed by anodic and cathodic surfaces in the micro-discharges onset.

In spite of many investigations carried out in the past, a consolidated model describing the physical phenomena occurring during the high voltage conditioning over long vacuum gaps is still missing in literature. Nevertheless the analyses of the present experimental results would suggest that the micro-discharges activity would depend on an cathode-anode interaction in which the local heating of the anode play a fundamental role in the micro-discharge onset.

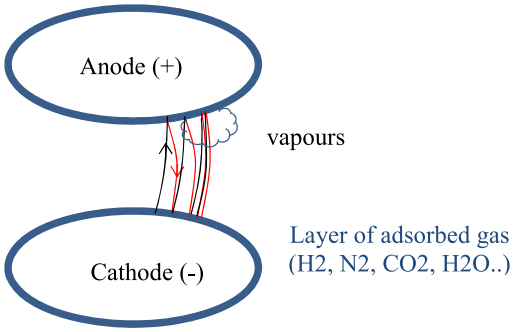

Figure 17. Sketch representing the cascade particles exchange between two generic electrodes, the red paths are the trajectories of the positive ions while the black one are the trajectories of the negative charged particles a layer of adsorbed gases cover the surface of both electrodes.

Probably the large anodic surface in front of the support connected to the negative power supply (on the left) is sufficient to limit the local temperature and the local outgassing. The same does not occur on the cantilever support connected to the positive power supply. Although the maximum temperature of the map shown in figure 7 does not exceed 30 °C, it is plausible that the temperature rise is the result of a local and transient heating not detectable by the IR camera. Actually the RGA plot of figure 6 is compatible with the measurements reported in [17]. The same type of emissions could be observed if the gas desorption had been thermally activated, nevertheless specific tests to confirm this hypothesis have not been done yet in our high voltage test stand.

A sketch representing a possible interpretation of the observed phenomena is shown in figure 17, Both electrodes are covered by a layer of adsorbed gases having a thickness of between 3 and 20 μm. The electrode shape could quickly focus the exchanged particles toward the accumulation points. Even though the latter generally are not located in the highest electric field area, the accumulation points can nevertheless collect the contribute of a large portion of electrode. The high flux of heat can rise locally the temperature enhancing the electrode sputtering, the desorption of the gases trapped in the layer on the metal vacuum interface and eventually promoting the microdischarge onset.

The mechanism so far described is one of the possible processes which limit the voltage holding of a generic system insulated by vacuum gaps. In the HVPTF such phenomena usually occur when $V+$ exceeds 120–150 kV. In this case an intense microdischarge activity can lead to a non-negligible dissipation of power, and, as a matter of facts, limits $V+_{MAX}$ below 210–220 kV, depending on the level of cleanness of the vacuum vessel.

6. Conclusions and proposal of a possible application

Experimental evidences concerning the existence of accumulation points during occurrence of micro-discharges have been observed during the high voltage conditioning of an electrostatic device insulated by large vacuum gaps. A mutual exchange of positive-negative charged particle is the mechanism which presumably causes this phenomenon and defines the position of the micro-discharge attractors.

The attractors regions due to the regenerative processes of charged particles between cathode and anode have been identified thanks to numerical ray-tracing simulations. The position of the attractors depends only on electrode shape and the ratios of applied voltages. A perturbation of the trajectories position by altering the voltage distribution has been sufficient to initiate the micro discharge occurrence.

The existence of phenomena able to concentrate the dissipation of power in specific location on the electrode surfaces during the high voltage conditioning in vacuum could be exploited in the development of neutrons sources applications.

The particles exchange could involve only electrons and positive ions or might be supported also by the formation of negative ions as postulated in [16]. In this second hypothesis, the phenomena would imply also the migration and the accumulation of material on the discharge attractors. Thus, the formation of accumulation points could be exploited in the development of neutrons sources applications.

Attempts to generate neutron sources by electrostatic accelerators by means of the bombardment of fast deuterium ions to hydrogen isotopes adsorbed in solid targets (such as titanium) have already been carried out for decades.

The following sentence has been extracted from a ’60 paper describing the development of a sealed-off vacuum tube used as sources of neutrons from fusion reaction [18].

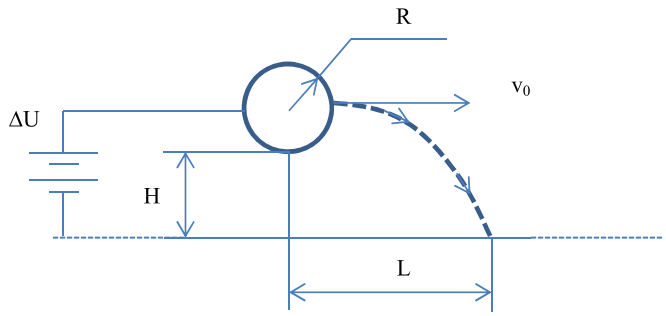

Figure A1. Quantities determining the throw L of a charged particle in an electrostatic field map, example of sphere plane geometry.

'It was found that ions could be produced from a vacuum arc struck between two electrodes of hydrogenated titanium, but the vacuum arc tended to strike erratically and at increasing higher threshold voltages'.

It is interesting to observe that the attempt to generate positive ions was limited by the high voltage conditioning of the hydrogenated titanium electrodes adopted in such specific test.

Considering the observations reported in the present paper, a further step forward in the development of neutrons sources applications could be the adoption of optimized system of electrodes to enhance the formation of attractor points. The accumulation of charged ions toward specific points could improve the efficiency of the neutron source limiting the loss of reactants sputtered by the accelerated ion collision.

The mechanism could be effective if the production of negative hydrogen ions on the cathodic surface is larger than the extraction of electrons, this could be obtained by combining two effects: seeding cesium at the cathode side and applying magnetic filter field (for electrons) in a region enclosing the attractor on the cathodic surface.

The proposal here reported is a speculation which can be verified only by dedicated experimental campaign.

Appendix

The independence of the classic trajectory upon mass, charge and even gap voltage can be done by means of the Buckingham Theorem [19].

Referring to figure A1, the distance L (the variable identifying the ending point of the trajectory) is a function of all the physical parameters governing the system.

$$L = f(m, q, v_0, H, R, \Delta U) \tag{2}$$

$$\Phi(L, m, q, v_0, H, R, \Delta U) = 0 \tag{3}$$

The number of fundamental physical units involved in equation (3) is 4, it corresponds to: [A],[s],[kg],[m] while the number of implicit variables in the same equation is 7. Equation (3) can be rewritten in term of $7–4 = 3$ dimensionless parameters as reported in equation (4):

$$\Phi'\left(\frac{L}{H}, \frac{m \cdot v_0^2}{q \cdot \Delta U}, \frac{R}{H}\right) = 0 \tag{4}$$

In case of $v_0 = 0$ [m/s] the trajectory depends only by R/H i.e. the trajectory depends only by the system geometry.

The conclusion is valid unless the motion is not relativistic, i.e. $q \cdot \Delta U \ll m \cdot c^2$, for accelerating voltages of our interest $\Delta U < 1e06\ [V]$ only electrons could be accelerated to relativistic speed because the condition $\frac{q}{m} \gg \frac{c^2}{\Delta U} = \frac{(3e08)^2}{1e06} = 9e10\left[\frac{C}{kg}\right]$ is satisfied only for electrons, however if the black trajectories shown in figure 14 had been calculated considering the relativistic equation of motion and the negative charged particles were electrons, the results of the calculations would not so different from those reported in figure 15.

ORCID iDs

N Pilan https://orcid.org/0000-0002-9849-8788
S De Ambrosis https://orcid.org/0000-0002-3186-232X
M Cavenago https://orcid.org/0000-0003-4486-687X
E Martines https://orcid.org/0000-0002-4181-2959

R Pasqualotto https://orcid.org/0000-0002-3684-7559
P Veltri https://orcid.org/0000-0002-0625-1201

References

[1] Hemsworth R S, Tanga A and Antoni V 2008 *Rev. Sci. Instrum.* **79** 02C109
[2] De Lorenzi A, Pilan N, Lotto L, Fincato M, Pesavento G and Gobbo R 2011 Proc. 26th symposium on fusion technology (SOFT-26) *Fusion Eng. Des.* **86** 742
[3] Latham R 1995 *High Voltage Vacuum Insulation* (San Diego, CA: Academic) Ch 2
[4] Latham R 2006 *High Voltage Vacuum Insulation, A New Perspective* (Milton Keynes: Author House)
[5] Cranberg L 1952 *J. Appl. Phys.* **23** 518
[6] Germain C and Rohrbach F 1968 *Vacuum* **18** 371
[7] Nishimori N, Nagai R, Matsuba S and Hajima R 2014 *Phys. Rev. S. T. Accel. Beams* **17** 053401
[8] Pilan N *et al* Numerical-experimental benchmarking of a probabilistic code for prediction of voltage holding in high vacuum Accepted on*IEEE Tran. Plasma. Sci.* (https://doi.org/10.1109/TPS.2017.2775246)
[9] Spagnolo S *et al* 2018 to be published in the*Proc. 28th Int. Symp. on Discharges and Electrical Insulation in VacuumSymposium (ISDEIV)*
[10] Spagnolo S *et al* 2018 Current signals and x- ray spectra analysis for a vacuum high voltage holding experiment *7th Int. Workshop on Mechanisms of Vacuum ARCs San Juan (Puerto Rico USA)* 20–4
[11] Siciliano E R, Ely J H, Kouzes R T, Schweppe J E, Strachan D M and Yokuda S T 2008 *Nucl. Instrum. and Meth. in Phys. Research* **594** 232
[12] Kramers H A 1923 *The London, Edinburgh, and Dublin Philosophical Magazine and Journal of Science* **46** 836
[13] Trump J G and Van De Graaff R J 1946 *J. Appl. Phys.* **18** 327
[14] Filosofo I and Rostagni A 1949 *Phys. Rev.* **75** 1269
[15] Klein O and Nishina Y 1929 *Y. Z. Physik* **52** 853
[16] Cavenago M, Antonini P, Veltri P, Pilan N, Antoni V and Serianni G 2010 Cascades of secondary particles in high voltage accelerators' *Comsol conference 2009, Boston, Milan, Bangalore: User Presentation and proceedings CD' (7pp) CD-ROM* ISBN 978-0-9825697-0-2 *(Comsol, Stockholm)*
[17] Diamond W T 1998 *J. Vac. Sci. and Tech.* **16** 720
[18] Gow J D and Pollock H C 1960 *Rev. Sci. Instrum.* **31** 235
[19] Buckingham E 1914 *Phys. Rev.* **4** 345